ORIGINAL ARTICLE

Micro–Computed Tomography Analysis of the Human Tuberculous Lung Reveals Remarkable Heterogeneity in Three-dimensional Granuloma Morphology

Gordon Wells[1], Joel N. Glasgow[2], Kievershen Nargan[1], Kapongo Lumamba[1], Rajhmun Madansein[3], Kameel Maharaj[3], Robert L. Hunter[4], Threnesan Naidoo[5], Llelani Coetzer[6], Stephan le Roux[6], Anton du Plessis[6], and Adrie J. C. Steyn[1,2,7]

[1]Africa Health Research Institute, University of KwaZulu-Natal, Durban, South Africa; [2]Department of Microbiology and [7]Centers for AIDS Research and Free Radical Biology, University of Alabama at Birmingham, Birmingham, Alabama; [3]Department of Cardiothoracic Surgery, Nelson Mandela School of Medicine, University of KwaZulu-Natal, Durban, South Africa; [4]Department of Pathology and Laboratory Medicine, University of Texas Health Sciences Center at Houston, Houston, Texas; [5]Department of Anatomical Pathology, National Health Laboratory Service, Inkosi Albert Luthuli Central Hospital, Durban, South Africa; and [6]Computed Tomography Scanner Facility, Central Analytical Facilities, Stellenbosch University, Stellenbosch, South Africa

ORCID IDs: 0000-0003-2328-5208 (G.W.); 0000-0001-9177-8827 (A.J.C.S.).

Abstract

Rationale: Our current understanding of tuberculosis (TB) pathophysiology is limited by a reliance on animal models, the paucity of human TB lung tissue, and traditional histopathological analysis, a destructive two-dimensional approach that provides limited spatial insight. Determining the three-dimensional (3D) structure of the necrotic granuloma, a characteristic feature of TB, will more accurately inform preventive TB strategies.

Objectives: To ascertain the 3D shape of the human tuberculous granuloma and its spatial relationship with airways and vasculature within large lung tissues.

Methods: We characterized the 3D microanatomical environment of human tuberculous lungs by using micro computed tomography, histopathology, and immunohistochemistry. By using 3D segmentation software, we accurately reconstructed TB granulomas, vasculature, and airways in three dimensions and confirmed our findings by using histopathology and immunohistochemistry.

Measurements and Main Results: We observed marked heterogeneity in the morphology, volume, and number of TB granulomas in human lung sections. Unlike depictions of granulomas as simple spherical structures, human necrotic granulomas exhibit complex, cylindrical, branched morphologies that are connected to the airways and shaped by the bronchi. The use of 3D imaging of human TB lung sections provides unanticipated insight into the spatial organization of TB granulomas in relation to the airways and vasculature.

Conclusions: Our findings highlight the likelihood that a single, structurally complex lesion could be mistakenly viewed as multiple independent lesions when evaluated in two dimensions. In addition, the lack of vascularization within obstructed bronchi establishes a paradigm for antimycobacterial drug tolerance. Lastly, our results suggest that bronchogenic spread of *Mycobacterium tuberculosis* reseeds the lung.

Keywords: *Mycobacterium tuberculosis*; computed tomography; imaging; bronchogenic spread; tree-in-bud

(Received in original form January 6, 2021; accepted in final form May 20, 2021)

Supported by NIH grants R01AI111940, R01AI137043, R61/33AI138280, R01AI134810, and R21A127182 (A.J.C.S.) and National Institute of Allergy and Infectious Diseases grant R01AI134810; Bill and Melinda Gates Foundation award OPP1130017 (A.J.C.S.); pilot funds from the University of Alabama at Birmingham Center for AIDS Research, Center for Free Radical Biology, and Infectious Diseases and Global Health and Vaccines Initiative (A.J.C.S.). The research was also cofunded by CRDF Global, the South African Medical Research Council, and a South African National Research Foundation Brazil, Russia, India, China, and South Africa multilateral grant (A.J.C.S.).

Author Contributions: Conceptualization and design: G.W., A.J.C.S. Lung tissue preparation: G.W., K.N., K.L. Micro–computed tomography scanning: A.d.P., S.I.R. High-resolution computed tomography: R.M., K.M. Pathology: T.N. Histopathology: K.N., K.L., R.L.H. Three-dimensional segmentation: G.W., A.d.P., L.C. Data integration: G.W., J.N.G., A.J.C.S. Writing of initial draft: G.W., J.N.G., A.J.C.S. Editing: J.N.G., A.J.C.S. Final draft: All authors. Figure preparation: G.W., A.J.C.S. All authors discussed the results and commented on the manuscript.

Correspondence and requests for reprints should be addressed to Adrie J. C. Steyn, Ph.D., Department of Microbiology, The University of Alabama at Birmingham, Birmingham, AL 35294-2172. E-mail: asteyn@uab.edu.

This article has a related editorial.

This article has an online supplement, which is accessible from this issue's table of contents at www.atsjournals.org.

Am J Respir Crit Care Med Vol 204, Iss 5, pp 583–595, Sep 1, 2021

Originally Published in Press as DOI: 10.1164/rccm.202101-0032OC on May 20, 2021
Internet address: www.atsjournals.org

At a Glance Commentary

Scientific Knowledge on the Subject: Histopathological analysis of necrotic granulomas caused by the bacterium *Mycobacterium tuberculosis* typically reveals a two-dimensional circular shape, which is intuitively assumed to be spherical or ovoid. When searching modern molecular literature on PubMed for explicit descriptions of tuberculosis granuloma morphologies, they are typically described as round, spherical, or ovoid.

What This Study Adds to the Field: We reveal that necrotic granulomas adopt complex, branched morphologies reminiscent of branched transport networks within the lung. In conjunction with findings from histopathological and immunohistochemical analysis, we conclude that these granuloma morphologies are largely shaped by bronchial and alveolar obstruction. Our use of three-dimensional segmentation highlights the possibility that a single, structurally complex lesion could be erroneously viewed as multiple independent lesions when evaluated in two dimensions. The potential for misinterpretation of the granuloma number, size, or position indicates that great care must be taken while interpreting "-omic" data derived directly from tuberculosis lesions, as conclusions will be influenced by the actual (but unknown) three-dimensional shape of the lesion. Furthermore, conclusions drawn regarding microenvironments surrounding what appear to be multiple granulomas could change if it were understood that a single complex lesion was under investigation.

In the 1940s and 1950s histopathological analysis was a mainstay for the investigation of tuberculosis (TB) disease when postmortem and resected human lung tissues were routinely available (1, 2). These pioneering studies have been largely forgotten and replaced by observations in nonhuman animal models that do not reproduce the pathology of human pulmonary TB.

The prevailing dogma in the TB field that granulomas form spherical or ovoid structures within the parenchyma (3–11) is based on two-dimensional (2D) histopathological studies of primary TB in animal models. Furthermore, very little is known about the three-dimensional (3D) structure of the necrotic TB granuloma, a distinctive feature of human TB. Because the cellular composition, vascularization, aeration, necrotic state (e.g., caseous, coagulative, fibrinoid), and bacillary burden are likely to affect the shape of the TB lesion, a deeper understanding of the morphological properties of the human TB granuloma in relation to the airways and vascular system is needed to more accurately inform preventive and therapeutic strategies.

Examination of TB lesions in three dimensions within large lung tissues could allow identification of disease-specific features and improve diagnosis. Histopathology is a destructive approach that provides excellent 2D results but can generate artifacts during fixation, slicing, and staining. Other practical limitations are low throughput and imperfect imaging of structures that extend beyond a typical 5-μm section, which have begun to hinder more detailed examination of human TB pathophysiology in the current antibiotic era, especially with the emergence of HIV. Other factors contributing to our limited understanding are a reliance on animal models, which do not fully recapitulate human TB phenotypes, and the paucity of routinely available resected human TB lung tissues (12). Tissues with post-primary TB lesions are even more rare. Therefore, high-resolution digital 3D imaging of TB lesions within large lung tissues will allow the detailed spatial analysis of complex microanatomical features specific to pulmonary TB and will improve our understanding of TB disease.

X-ray computed tomography (CT) is invaluable for nondestructive imaging of tissue in medical diagnosis (13, 14). Recent studies in patients with TB using positron emission tomography (PET)–CT have reported substantial heterogeneity in metabolic uptake of fluorodeoxyglucose F 18 ($[^{18}F]$FDG), a proxy for TB lesions. Notably, one-third of patients showed new lesions after 1 year of anti-TB drug therapy (15), suggesting that *Mycobacterium tuberculosis* disseminates within the lung during treatment. Concerningly, it seems to have been forgotten that in the preantibiotic era, post-primary TB was known as bronchogenic TB because it spreads through the bronchi rather than the lymphatics or bloodstream (1, 16, 17), which remains well known by radiologists (18, 19). To our knowledge, no study has reported the use of high-resolution micro-CT (μCT) to examine bacterial disease in human lungs.

To better understand pulmonary TB, new imaging techniques are needed that can improve on and complement standard modalities such as high-resolution CT (HRCT) and histology. Here, we exploited μCT to characterize the structure, distribution, and volume of necrotic lesions relative to the airways and vasculature and confirmed our findings by using histopathology and immunohistochemistry (IHC). Some of the results of these studies have been previously reported in the form of a preprint (https://doi.org/10.1101/2020.06.14.149898).

Methods

Ethics and Human Subjects

This study was approved by the University of KwaZulu-Natal Biomedical Research Ethics Committee (class approval study number: BCA 535/16). Patients undergoing lung resection for TB (study identifier: BE 019/13) were recruited from King DinuZulu Hospital Complex, a tertiary center for patients with TB in Durban, South Africa. *M. tuberculosis*–infected human lung tissues are routinely obtained after surgery for removal of irreversibly damaged lobes or lungs (bronchiectasis and/or cavitary lung disease). Written informed consent was obtained from all participants. All patients undergoing lung resection for TB had completed a full 6- to 9-month course of anti-TB treatment or up to 2 years of treatment for drug-resistant TB. Patients were assessed for the extent of pulmonary disease (cavitation and or bronchiectasis) via HRCT. The fitness of each patient to withstand a thoracotomy and lung resection was determined by using the Karnofsky score, 6-minute-walk test, spirometry, and arterial blood gas measurement. Assessment of patients with massive hemoptysis included their general condition, effort tolerance before hemoptysis, arterial blood gas measurement, serum albumin concentration, and HRCT imaging of the chest. On gross assessment, all pneumonectomies or lobectomies were bronchiectatic, hemorrhagic, variably fibrotic, and atelectatic and contained visible tubercles (*see* Table E1 in the online supplement).

Sample Preparation

Before μCT or histology, all samples were fixed in 10% buffered formalin for at least 14 days. All samples were contrast stained with iodine by immersing the samples in 2.5% Lugol's solution for 1–5 days depending on sample size. For μCT scanning, samples were mounted on or in 50-ml falcon tubes or larger, sealed plastic containers by using a combination of cellophane tape and floral foam. Samples were lodged above a bath of 10% formalin in the bottom of the container with floral foam and lodged between the walls to prevent shifting of the sample. The low density of the foam also enables easy deletion from the reconstructed volume during subsequent visualization and analysis. When necessary, the containers (50-ml tubes without gaskets) were then sealed with parafilm for the duration of the scan to prevent desiccation. Before mounting, samples were rinsed with water and dabbed dry to remove excess staining solution.

μCT Scanning

A General Electric Phoenix v|tome|xL240 system was used for μCT (2,024 × 2,024–pixel image, 16-bit depth) with a resolution range of 12.0–80.0 μm. Although the instrument is capable of a submicrometer resolution for small samples, none of the samples analyzed in this study were small enough. All samples were scanned over 360°. Voltage varied between 8 and 160 kV, the current varied between 180 and 400 μA, and scanning times ranged from 2,700 to 3,000 seconds. For all scans, a tungsten target was employed.

Results

μCT Characterization of the Human TB Granuloma

In Durban, South Africa, *M. tuberculosis*–infected human lung tissues are routinely obtained after resection of irreversibly damaged lung regions exhibiting bronchiectasis and/or cavitary lung disease (20, 21). We analyzed lung specimens obtained from 17 subjects (Table E1). Specimens displayed typical signs of bronchiectasis and contained tubercles of varying volume and shape. Representative sections of the cavitational and parenchymal abnormalities were used for imaging or histopathology studies.

To improve the clinicopathological analysis of TB, we sought to establish a correspondence between radioopacity and pathological features within lesions that permitted 3D reconstruction. TB lesions have pathological features that can evolve over decades (1, 2). Although these structures likely represent unique immunopathological microenvironments, their contribution to TB disease and *M. tuberculosis* persistence is poorly understood. This is partly due to the inability of 2D histology to adequately characterize these deformities. We scanned a contrast-stained lung tissue sample exhibiting caseous necrosis at a 12.0-μm resolution (Figures 1A and 1B). Segmentation identified distinct regions that matched blood vessels and necrotic lesions. The identification of lesions and vasculature with μCT was confirmed by histology with hematoxylin and eosin (H&E) and Masson's trichrome staining (Figures 1C and 1D), revealing several necrotic lesions and evidence of fibrosis. Inspection of the lesions revealed common radioopacity patterns, which we confirmed quantitatively by plotting relative X-ray attenuation (electron density) across representative sections (Figures 1E and 1F). The necrotic lesions are surrounded by a dark outer layer of radioopacity (Figures 1G–1J) corresponding to lamellar fibrosis by H&E (Figures 1K–1N) and trichrome staining (Figures 1O–1R). The necrotic region exhibits a light border (Figures 1E–1J, and Figure E1 in the online supplement), which is likely derived from the former bronchial epithelium. This corresponds to a more intensely stained border in H&E and trichrome staining (Figures 1K–1R) surrounding a mass of less electron-dense necrotic material. Hence, we were able to establish a correlation between pathophysiological features and differences in radioopacity. In addition, in one lesion (Figure 1G), μCT revealed two internal lobes that were not apparent in the corresponding histopathology (Figures 1K and 1O), further emphasizing the potential of μCT to identify unusual pathological features. These data demonstrate that μCT can effectively identify TB lesions on the basis of their distinct electron density features associated with necrosis and fibrosis.

Segmentation and Spatial Distribution of Granulomas in the Human Lung

Although conventional histopathology provides detailed information on very small areas of interest, it cannot contextualize TB lesions within the overall lung architecture, thereby limiting accurate assessment of the overall distribution and shapes of lesions. Human PET–CT imaging studies have shown that individual TB lesions evolve independently. However, because increased metabolic uptake of [^{18}F]FDG is a proxy for inflammation (15), it does not demonstrate the early noninflammatory lesions of TB that precede formation of tuberculous pneumonia, cavitation, and granulomas and reveals inflammation from other causes besides TB. In addition, because the term "lesion" may refer to any tissue abnormality (e.g., cavities, mycetoma, nodule- and pleura-based infiltrates, fibrotic nodules, patchy consolidation, etc.) and because the early and very late lesions of human TB have little inflammation, we caution against comparing the diverse pathologies (lesions) identified by PET–CT (15) with the granulomas characterized in this study. Whereas the resolution of PET–CT does not allow accurate 3D segmentation that can reveal granuloma morphology, μCT has the potential to accurately define granuloma structure and spatial orientation relative to sources of nutrients, anti-TB drugs, and oxygen. To contextualize TB lesions relative to the vasculature and airways, we scanned a large slice of TB lung at a 52.0-μm resolution (Figures 2A and E2, Video E1). The use of 3D segmentation showed that larger necrotic lesions are oriented with a directionality similar to that of the vasculature and bronchial networks (Figure 2B). Notably, multiple lesions were transected during sectioning of the tissue (Figure 2C), revealing that the lesions have more complex structures that continue beyond the sectioning plane. In addition, airways were absent in areas where lesions predominated, suggesting that these lesions are the remnants of previously obstructed airways.

Surface area rendering of a subsection of this sample distinctly identified lesions, blood vessels, and airways (Figure 3A), and 3D segmentation revealed six lesions (Figure 3B). High signal intensity of erythrocytes permitted rapid, albeit partial, reconstruction of the vasculature (Figure 3C). Vascular destruction, also observed in Figure 2B, contributes to interstitial hemorrhage, resulting in nutrient and O_2 deprivation, which likely exacerbates the host pathophysiology. A considerable degree of hemorrhaging was observed with segmentation by thresholding, generating large volumes obscuring the lesions and airways (Figure 3C). We measured distances between the intact vasculature and necrotic lesions because their proximity would impact lesion development and morphology. The

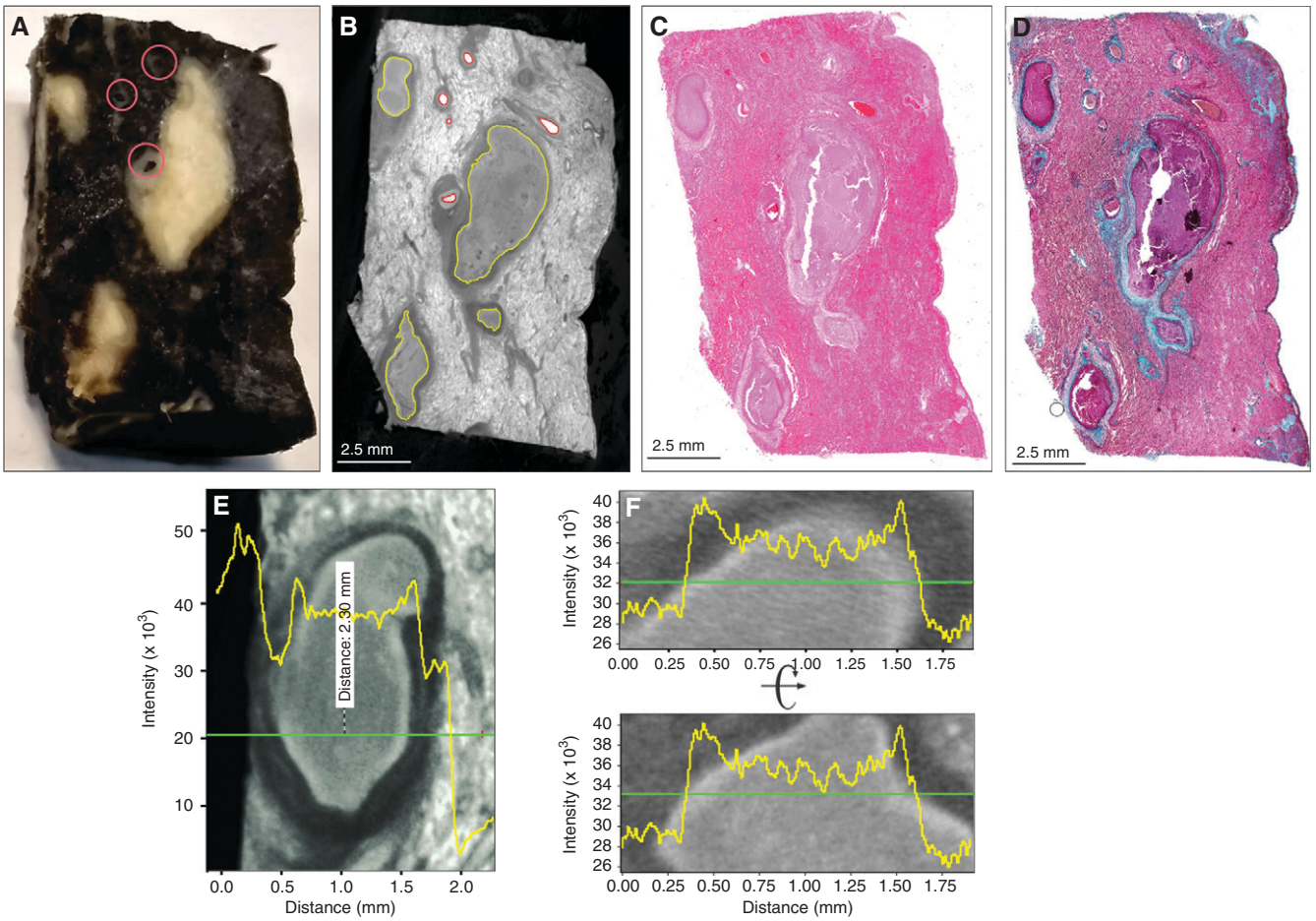

Figure 1. Micro computed tomography (μCT) and histology of human tuberculosis lung with caseous necrotic granulomas. (*A*) Gross image of tissue exhibiting caseous necrosis. Pink circles indicate blood vessels. (*B*) μCT (12.0-μm resolution) of tissue in *A*, showing caseous necrosis (yellow outlines) and blood vessels (red outlines). (*C*) Hematoxylin and eosin histology of *B*. (*D*) Masson's trichrome histology of *B*. (*E–J*) Necrotic regions have a "halo-like" appearance with a slightly brighter outer shell (green arrows) surrounding a slightly darker interior (yellow arrows). The green arrows indicate denser necrotic material likely derived from a necrotic bronchial epithelium (*see also* Figure E1 in the online supplement). Necrotic regions are surrounded by a dark border (blue arrows). (*E* and *F*) Typical X-ray opacity profile (yellow line graph) across necrotic granulomas measured along the green axis. X-ray attenuation is proportional to intensity and is visualized inversely, with denser regions appearing brighter. Intensity is a combination of tissue density and iodine (contrast stain) affinity. Dark fibrotic regions are followed by a slightly more opaque ring that surrounds the (lighter) lesion. (*G–J*) Representative μCT images of caseous necrotic lesions. Dotted lines indicate region borders. (*K–N*) Hematoxylin and eosin and (*O–R*) Masson's trichrome histology corresponding to *G–J* reveal the darker border (blue arrows) surrounding the necrotic regions corresponding with fibrotic tissue. Boxed regions in *I, M,* and *Q* are shown at high magnification in *J, N,* and *R*, respectively. Scale bars: *B–D*, 2.5 mm; *G–I*, 1 mm; *J*, 500 μm. Reprinted by permission from Reference 41.

maximum O_2 diffusion distance from blood vessels is 100–200 μm (22–24), and metabolic zonation may account for spatial lesion heterogeneities (25). Although histopathological analyses have shown that distances between TB lesions and the vasculature can exceed 200 μm, this could be influenced by the sectioning plane. For example, by using 3D segmentation, we observed that the vasculature followed the curvature of the lesions spatially. The distances between blood vessels and lesions ranged from 0.5 to 1.4 mm (Figures 3D and E3). Hence, the curvature of lesions must be considered to accurately measure these distances, which are important for understanding the delivery of nutrients, drugs, and O_2 to bacilli (Figure E4) and immune cells in and around the lesion.

Our results show that integration of conventional histopathological methods with μCT can be used to identify pathological features such as lesion volume, 3D structure, and intralesional features in the context of a whole-lung slice. The spatial organization of lesions relative to the pulmonary vasculature is particularly important because vascular destruction will reduce delivery of anti-TB drugs, O_2, and nutrients. Importantly, the lack of airways and the directionality of lesions suggest that some TB lesions observed by using conventional histopathology are likely cross-sections of obstructed airways that are cylindrical, not spherical. Lastly, in contrast to histopathology that provides a snapshot of disease pathology in a very small area, 3D scanning of a whole-lung section provides detailed evidence of the spatial distribution and complexity of lesions in relation to the airways and vascular system. Hence, μCT can improve our understanding of the pathophysiological mechanisms of TB and a poor response to anti-TB drugs.

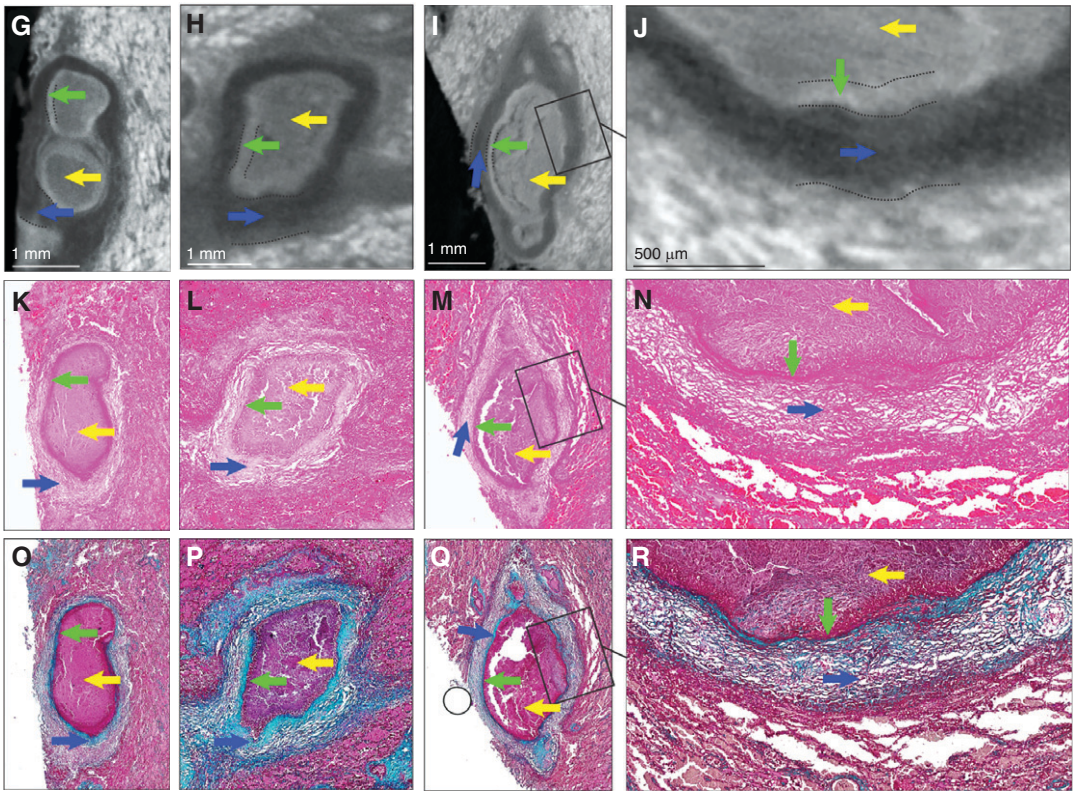

Figure 1. (*Continued*).

The Morphology of TB Granulomas Is Shaped by the Bronchi

Here, we characterized the spectrum of granuloma structures (Figure 4A) obtained from the sample in Figure 2 in more detail. In contrast to the widely held assumption that TB granulomas are nearly spherical, segmentation of caseous necrotic lesions revealed remarkable morphological heterogeneity and complexity (Figure 4A). Of the 40 granulomas segmented in Figure 2, multiple highly branched structures were observed. The radius (of the smallest enclosing sphere) of these lesions ranged from 0.5 to 7 mm. Smaller lesions were more spherical, whereas larger lesions were branched with lower sphericity, ranging from 0.23 to 0.6 (1.0 is a perfect sphere) (Figure 4B). Smaller lung samples were scanned at a higher resolution, further revealing the complexity of the lesion microenvironment (Figures 4C–4I, Videos E2–E5). A section taken from the sample in Figure 2A contains a complex ginger root–like structure (Figures 4C–4F, Video E3). A second sample from a different patient revealed small lobular regions resembling the buds of the "tree-in-bud" signature often seen in HRCT scans (18, 25) of post-primary TB and bronchial obstruction (Figures 4G–4I, Video E4). We observed severe hemorrhaging, as indicated by the high-intensity areas in Figures 4C. Segmentation of the strands of high intensity reveals an intricate vasculature that surrounds lesions in both samples (Figures 4D, 4E, and 4H). Both granuloma structures in Figures 4C–4F and 4G–4I continue beyond the beyond the scanned view, indicating that the granulomas are larger and more complex.

To explore the spatial relationship between bronchi and TB lesions, we segmented the volumes surrounding the lesions, airways, and vasculature in Figure 2B. The use of μCT revealed diseased regions of similar radioopacity (dark area) surrounding the necrotic granulomas, airways, and blood vessels (Figure 5A). Segmentation of this pathology revealed that it surrounds and connects granulomas with airways (Figure 5B), suggesting that the shape of TB lesions is dictated by bronchi (Video E5). Morphological lesion heterogeneity was independently validated by using thorough μCT characterization of a separate whole-lung slice containing numerous granulomas (Figure E5).

Overall, our 3D data demonstrate that TB granulomas have remarkable morphological diversity. Whereas 2D histopathology sectioning typically reveals "round" granulomas that are inferred to be spherical, as observed by Rich (1) and Canetti (2), our results point to more complex cylindrical or branched-type morphologies, with lesions being connected to and shaped by the small airways.

Immune-Cell Infiltration of Bronchi Shapes the TB Granuloma

Our μCT data suggest that TB granuloma morphology is shaped by the small airways (Figures 2, 4, and 5, Video E5). We investigated this further by examining immune-cell infiltration and subsequent blockage of airways by using histopathology and IHC. We confirmed the presence of *M. tuberculosis* bacilli within neutrophils (Figure E6), within macrophages (Figure E7), extracellularly within alveoli (Figure E7), and within an obstructed bronchus (Figure E8). In highly consolidated areas of the tuberculous lung (Figures 6A, 6B, and E9), we identified patterns of epithelial-cell remnants consistent with obstructed small airways, as indicated by cytokeratin 7 and 3-mercaptopyruvate sulfurtransferase staining, which identifies epithelial cells (26) (Figures 6C–6F). These findings demonstrate that immune-cell

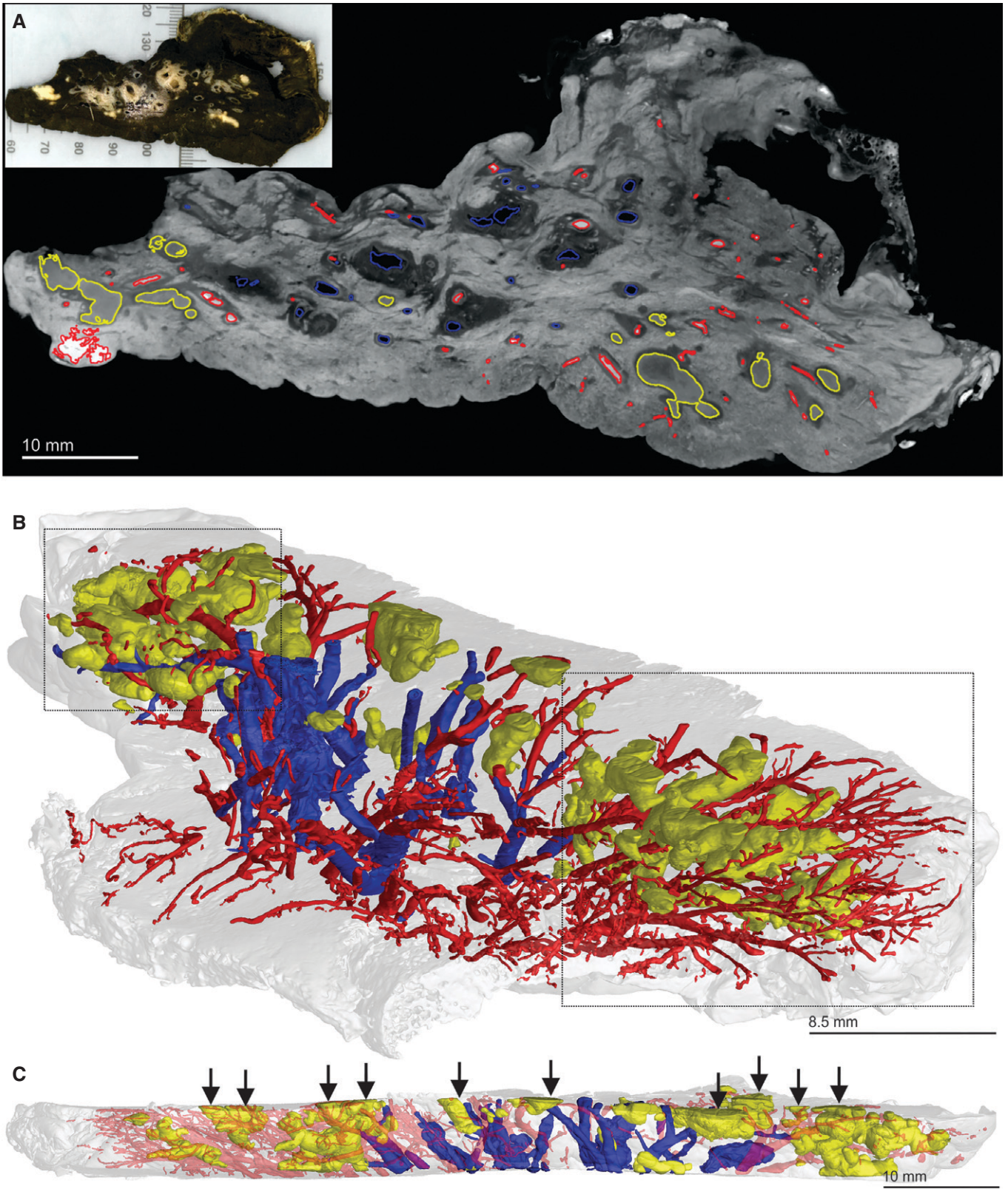

Figure 2. Micro computed tomography and segmentation of a human tuberculosis lung slice. (*A*) Two-dimensional slice of micro computed tomography (52.0-μm resolution) of an upper lobe. Necrotic granulomas (yellow), bronchi and/or bronchioles (blue), and the vasculature (red) are outlined. The inset shows the gross image of the lung slice (*see also* Figure E1). (*B*) Lung slice in *A* at an angle to best illustrate the three-dimensional organization of granulomas (yellow), bronchi and/or bronchioles (blue), and the vasculature (red). Complex necrotic granulomas are oriented similarly to the airways and vasculature. The two boxed areas show the absence of airways in regions where granulomas predominate, suggesting replacement through bronchial obstruction. (*C*) Side view of *A* with transected granulomas indicated by vertical arrows. Scale bars: *A* and *C*, 10 mm; *B*, 8.5 mm. Reprinted by permission from Reference 41.

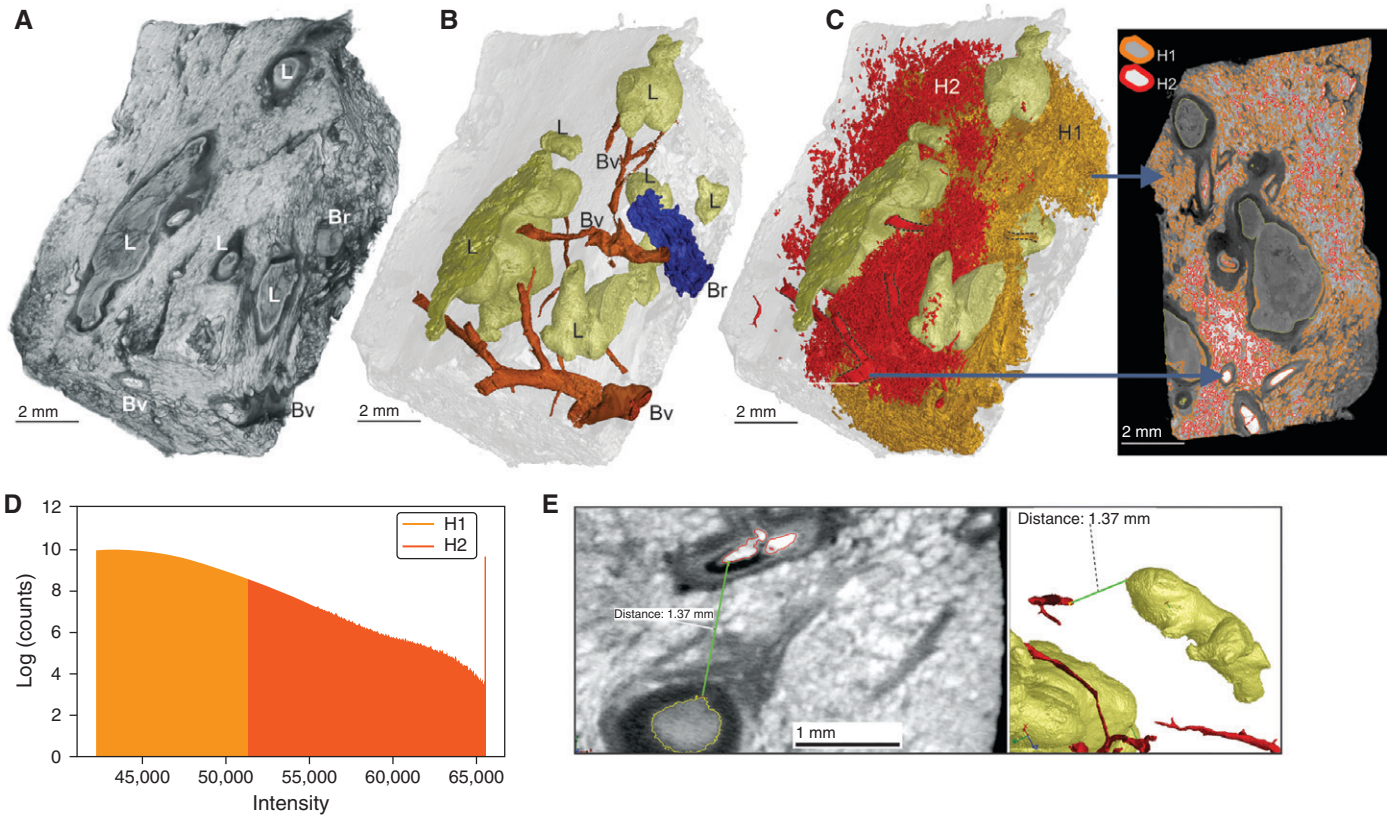

Figure 3. Heterogenous caseous granuloma morphology and surrounding vasculature. (*A*) Tissue sample exhibiting caseous necrotic granulomas. ScatterHQ (VG Studio) rendering of surface electron density was used. (*B*) Three-dimensional (3D) segmentation and two-dimensional slice of blood vessels (Bv; red), bronchioles and/or airways (Br; blue), and truncated lesions (L; yellow). (*C*) The 3D segmentation of lesions (yellow) and hemorrhaging (red and orange). Bv and nearby regions of hemorrhaging have a relatively high signal intensity, with decreasing intensity being demonstrated further away from the Bv. By selecting all regions above a high-intensity threshold (H2; red), hemorrhaging (including intact vasculature) can be quickly segmented. The selection of regions at a lower threshold (H1; orange), which includes H2, also selects other components outside the hemorrhaged region (e.g., within the lesions). The H1 region shown as partially clipped to reveal the H2 region. (*D*) Intensity distributions of H1 (orange) and H2 (red) regions demonstrating that the H2 region is included in the H1 region. (*E*) Representative micro–computed tomography slice of segmented regions from *A* demonstrating the distances between the (curved) granulomas and the vasculature. The 3D visualization allows for more accurate distance determination compared with histology, which will often not capture the minimum distance. Scale bars: *A*–*C*, 2 mm; *E*, left image, 1 mm. Reprinted by permission from Reference 41.

recruitment during early inflammation obstructs the small airways, which subsequently develop into granulomas surrounded by epithelial cells (Figure E10). In less consolidated areas, macrophages, neutrophils, and lymphocytes obstruct alveoli (Figure 6G), leading to independent and coalesced early granuloma formation (Figure 6H).

We next examined the contribution of innate and adaptive immune cells to bronchial and alveolar obstruction. Histopathological appraisal of lung tissue from several patients with TB identified numerous obstructed bronchi containing immune cells (Figures 6I–6L). We identified an abundance of myeloid-cell populations, indicated by positive staining of MPO (myeloperoxidase), LCA (leukocyte common antigen), and CD68 and histopathology (Figures 6M–6O, E9, and E11). We observed positive staining of T-cell lymphocytes ($CD4^+$ and $CD8^+$) (Figures 6P, 6Q, E11D, and E11E) inside and outside an obstructed bronchus and observed B cells ($CD20^+$) (Figures 6R and E11F) that dominate the area around the bronchus. Notably, in the consolidated diseased areas in Figures 6M–6R (boxes), IHC provides clear evidence of myeloid-cell and lymphoid-cell infiltration (Figures E11A–E11F), which is consistent with the consolidation shown in Figures 6A–6F. Lastly, we observed necrotic debris and immune cells from TB granulomas spilling into a bronchus (Figures 7A and 7B), providing compelling evidence that expansion of necrotic lesions along the airway network can shape granuloma structure and disseminate *M. tuberculosis*. Importantly, these granulomas are surrounded by foam cells (Figure E12), which is consistent with previous studies showing that obstructive lobular pneumonia softens lung tissue (i.e., caseous necrosis), which is then coughed up, leading to cavitation (12, 27).

Finally, our histopathology and IHC data are consistent with μCT imaging in demonstrating that the recruitment and expansion of immune cells in the airways, eventually followed by necrosis, contribute to blockage of the airways and ultimately contribute to granuloma morphology. These findings establish a foundation for a more accurate understanding of the 3D granuloma structure, bronchogenic spread to reseed the lung, and cavity formation.

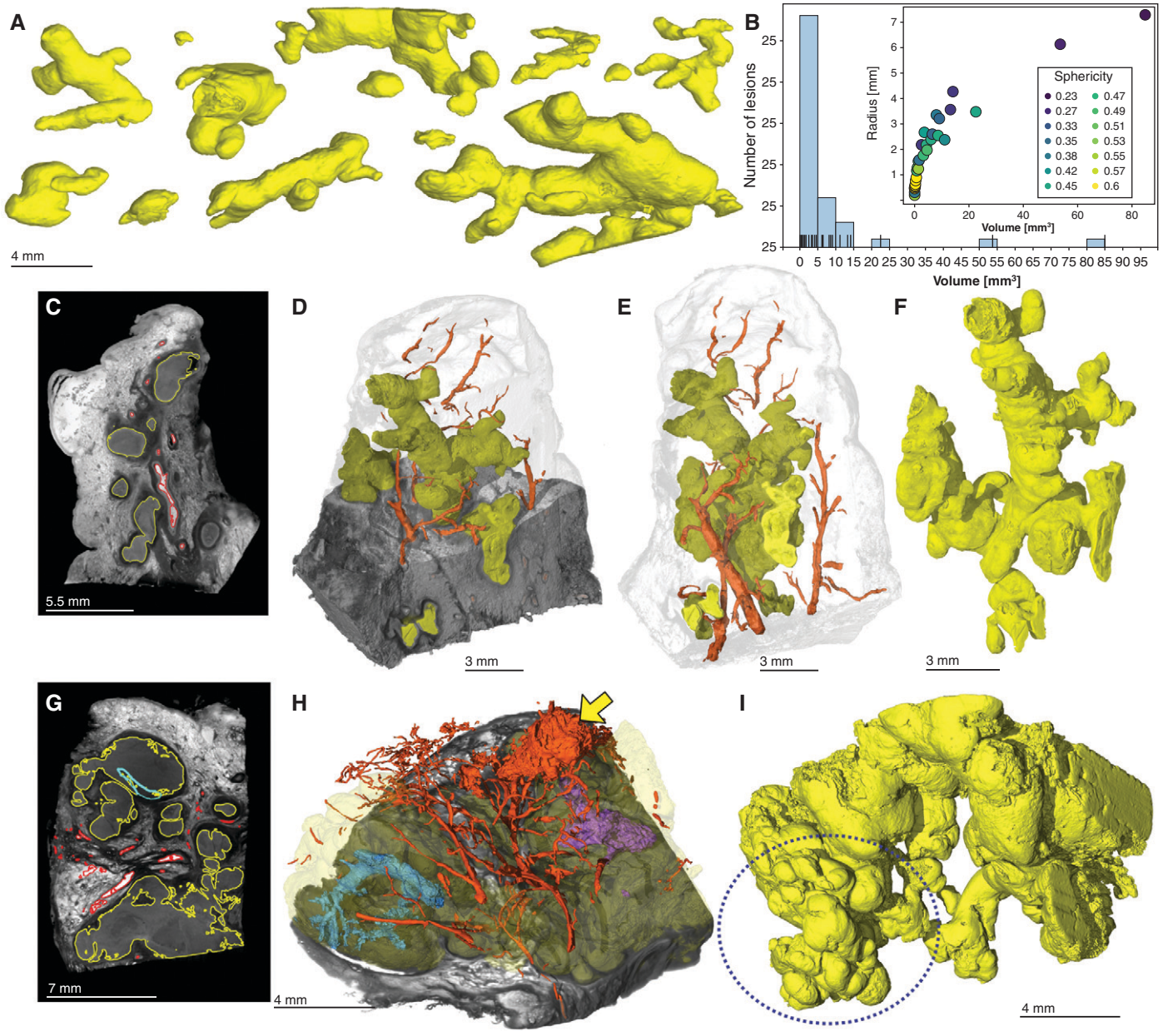

Figure 4. Granuloma morphology heterogeneity and surrounding vasculature. (*A*) The morphology of necrotic granulomas in tuberculosis ranges from small nodules (millimeter scale) to large, branched structures (centimeter scale) within a lung sample. (*B*) Relationship between lesion size and shape. Sphericity is the ratio of the surface area of a sphere to the surface area of the lesion when the sphere and lesion have equal volumes. Smaller granulomas tend to be nodular (higher sphericity), whereas larger granulomas exhibit more complex shapes with lower sphericity. (*C–F*) Micro computed tomography of the tip cut from the sample in Figure 2A. (*C*) Two-dimensional slice of tissue presumably containing multiple granulomas. (*D*) Three-dimensional (3D) rendering X-ray cutaway of the lesion (yellow) and vasculature (red) demonstrating a single large granuloma. (*E*) The 3D rendering of granulomas (large and small; yellow) and vasculature (red) segmentation in relation to the sample surface. (*F*) The 3D rendering of a granuloma (yellow) only. (*G–I*) Micro computed tomography of a necrotic tissue sample from a different patient. (*G*) Two-dimensional slice showing necrotic granulomas (yellow), intragranulomatous abnormalities (cyan), and the vasculature (red), which are outlined. (*H*) The 3D rendering and X-ray cutaway of granuloma (yellow) and vasculature (red) segmentation. The yellow arrow indicates hemorrhaging, and the purple and turquoise structures indicate obliterated airways. (*I*) The 3D rendering of granulomas (yellow) only. The dotted circle indicates an area resembling a tree-in-bud signature. Scale bars: *A*, 4 mm; *C*, 5.5. mm, *D–F*, 3 mm; *G*, 7 mm; *H* and *I*, 4 mm. Reprinted by permission from Reference 41.

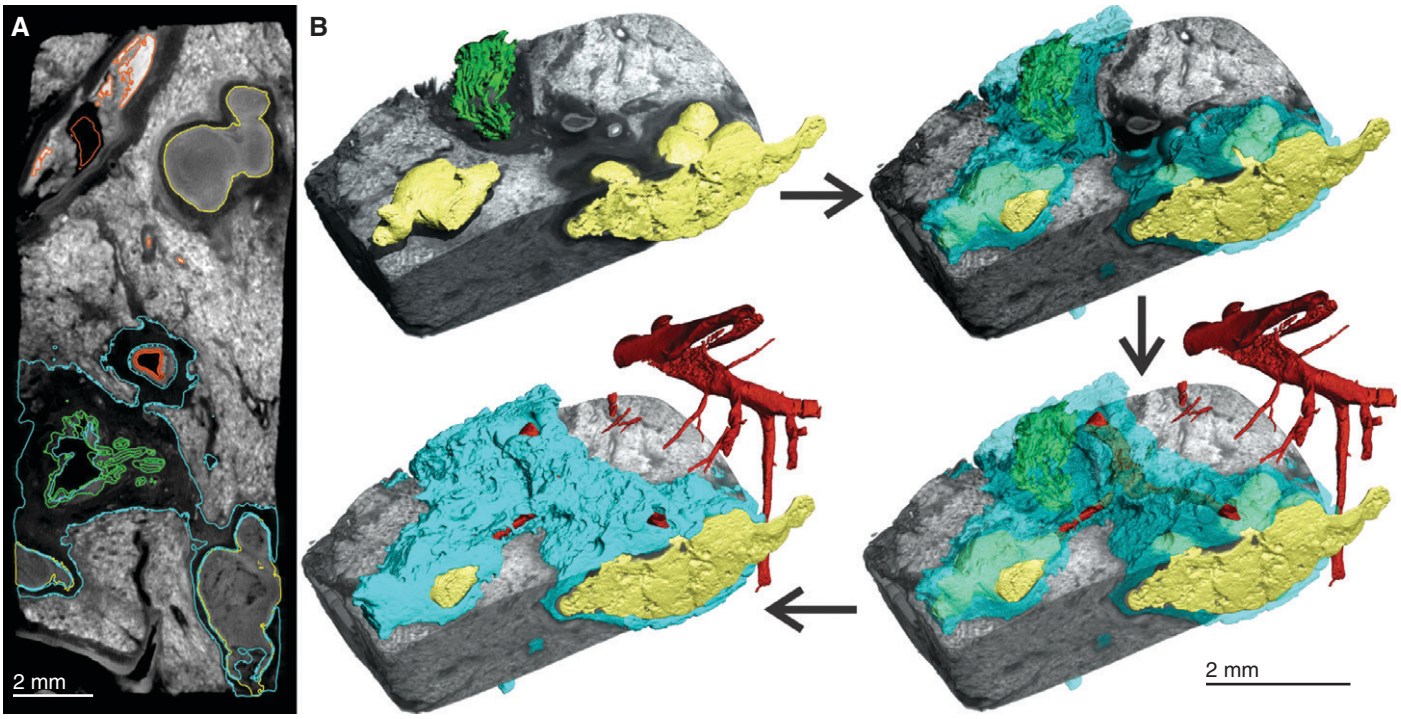

Figure 5. Segmentation of necrotic granulomas demonstrating their connection with the airway. (*A*) Two-dimensional slice of tissue containing multiple granulomas. Necrotic granulomas (yellow), the vasculature (red), and the bronchus (green) are outlined. (*B*) Three-dimensional rendering of necrotic granulomas, the vasculature, and the bronchus (color coding is the same as in *A*) demonstrating the granuloma/vasculature/airway network (cyan) in decreasing transparency from *A*. Note how segmentation of the diseased tissue of similar radioopacity (dark area) surrounds and connects necrotic granulomas and airways, and also connects blood vessels to some extent, suggesting that the airways help shape the granuloma structure. *See also* Video E5 in the online supplement. Scale bars, 2 mm.

Discussion

Although conventional histological methods have been the gold standard for appraising TB disease pathology for over 100 years, there is a need to address the multidimensionality of diseased tissue by using high-resolution imaging. In the 1940s and 1950s, the paradigm of human TB disease was shaped by the histopathological interpretations of Arnold Rich (1), George Canetti (2), and Edgar Medlar (28, 29) when postmortem and resected human lung tissues were routinely available. Concerningly, much of our current understanding of TB pathology is based on animal models that do not reproduce the full spectrum of disease as it occurs in humans. With the emergence of HIV and its synergism with TB, drug-resistant *M. tuberculosis*, and widespread access to anti-TB drugs (30–32), it is reasonable to suppose that TB pathology phenotypes have changed. Here, μCT imaging has provided new insight into the morphologies of human necrotic TB lesions, revealing branched and cylindrical structures with large variations in volume, size, and spatial organization, and suggests that lesions are shaped by the small airways. These findings are in contrast to the current dogma that granulomas are spherical, an understandable conclusion based on conventional histopathology. Our findings exemplify how 3D visualization of TB disease pathophysiology within small and large lung sections improves our understanding of the diversity of granuloma shapes and how bronchogenic dissemination contributes to TB disease. Hence, our findings provide a rationale for considering aerosolized anti-TB drug delivery. This approach could allow delivery of high, local concentrations of drugs directly into granulomas or cavities in the lung, possibly reducing treatment times, systemic dosing, and toxicity (33).

A significant advance is the application of 3D segmentation to the microarchitecture of whole sections of the tuberculous lung, which provides detailed insight into the spatial relationship among TB granulomas, the airways, and the pulmonary vasculature. To our knowledge, such findings have not yet been reported for any bacterial pulmonary pathogen. Several unexpected discoveries about TB granulomas were made. First, the TB granuloma represents a spectrum of complex, branched-type morphologies and is shaped by the small airways. Because the prevailing presumption has been that the granuloma is spherical (3–11), these observations may aid in elucidating the process of granuloma formation, which is poorly understood. The use of 3D segmentation highlights the possibility that a single complex lesion could be erroneously viewed as multiple independent lesions when evaluated in two dimensions. The potential for misinterpretation of the granuloma number, size, or position suggests that care must be taken while interpreting "-omic" data derived from TB lesions, as erroneous conclusions may be drawn because of the unknown shape of the lesion. For example, conclusions about microenvironments surrounding apparent multiple granulomas could change if they were known belong to a single complex lesion.

Second, the ability to quantify lesion size, volume, morphology, and spatial distribution within whole-lung slices represents a significant advance compared with histopathology. With respect to the granuloma

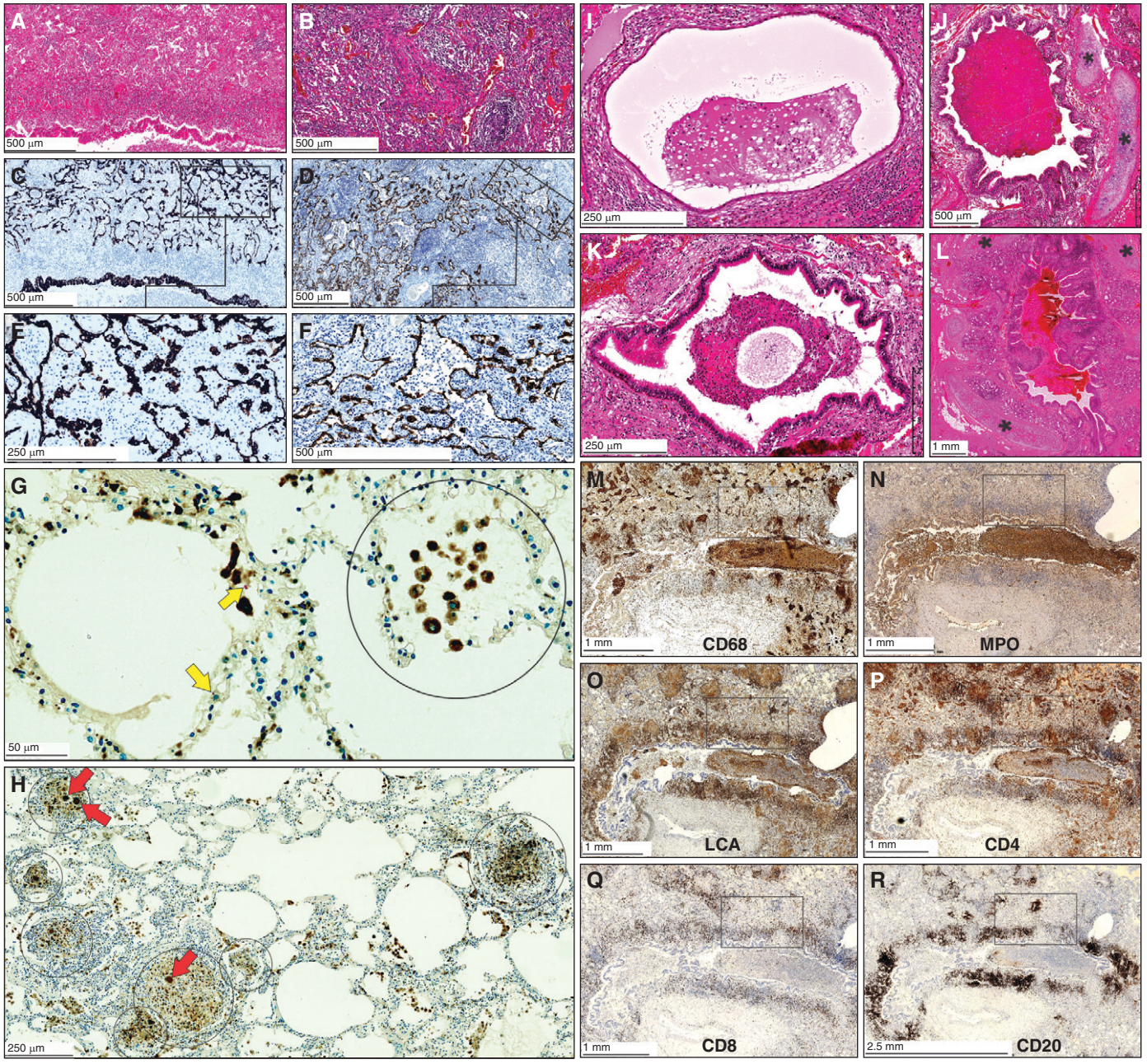

Figure 6. Histopathology of the small airways of *Mycobacterium tuberculosis*–infected human lungs demonstrating bronchial obstruction. (*A* and *B*) Low-power magnification of hematoxylin and eosin staining of the lung parenchyma. (*C* and *D*) Low-power and (*E* and *F*) medium-power magnification of epithelial staining in the adluminal layer demonstrating alveolar consolidation (*C* and *E*, CK7; *D* and *F*, 3MPST). (*G* and *H*) Combined CD68 immunohistochemistry and Ziehl–Neelsen staining demonstrating the presence of macrophages and *M. tuberculosis,* respectively. Circled areas indicate alveoli filled with macrophages, and red arrows indicate giant cells. Yellow arrows indicate *M. tuberculosis*. (*I*–*L*) Hematoxylin and eosin staining of bronchial obstruction. Asterisks indicate cartilage. (*M*–*R*) Immunohistochemistry of myeloid cells and lymphocytes. For high-power images of boxed areas in *M*–*R*, *see* Figures E8 and E10 in the online supplement. Scale bars: *A*–*D*, *F*, and *J*, 500 μm; *E*, *I*, *K*, and *H*, 250 μm; *G*, 50 μm; *L*–*Q*, 1 mm; *R*, 2.5 mm. LCA = leukocyte common antigen; MPO = myeloperoxidase.

number, early studies have shown that lesions produced via the bloodstream are more numerous and smaller than those generated by inhalation (2). In addition, granulomas of hypersensitive patients are bigger than those of less sensitized patients and increase in size over time (2). Seminal human PET–CT imaging studies suggest that individual TB lesions evolve independently in humans (15), and it is tempting to relate these gross lesions with histological granulomas. However, increased uptake of [^{18}F]FDG, predominantly by myeloid cells, is an indicator of glucose metabolism, which is associated with inflammation and used as a proxy for

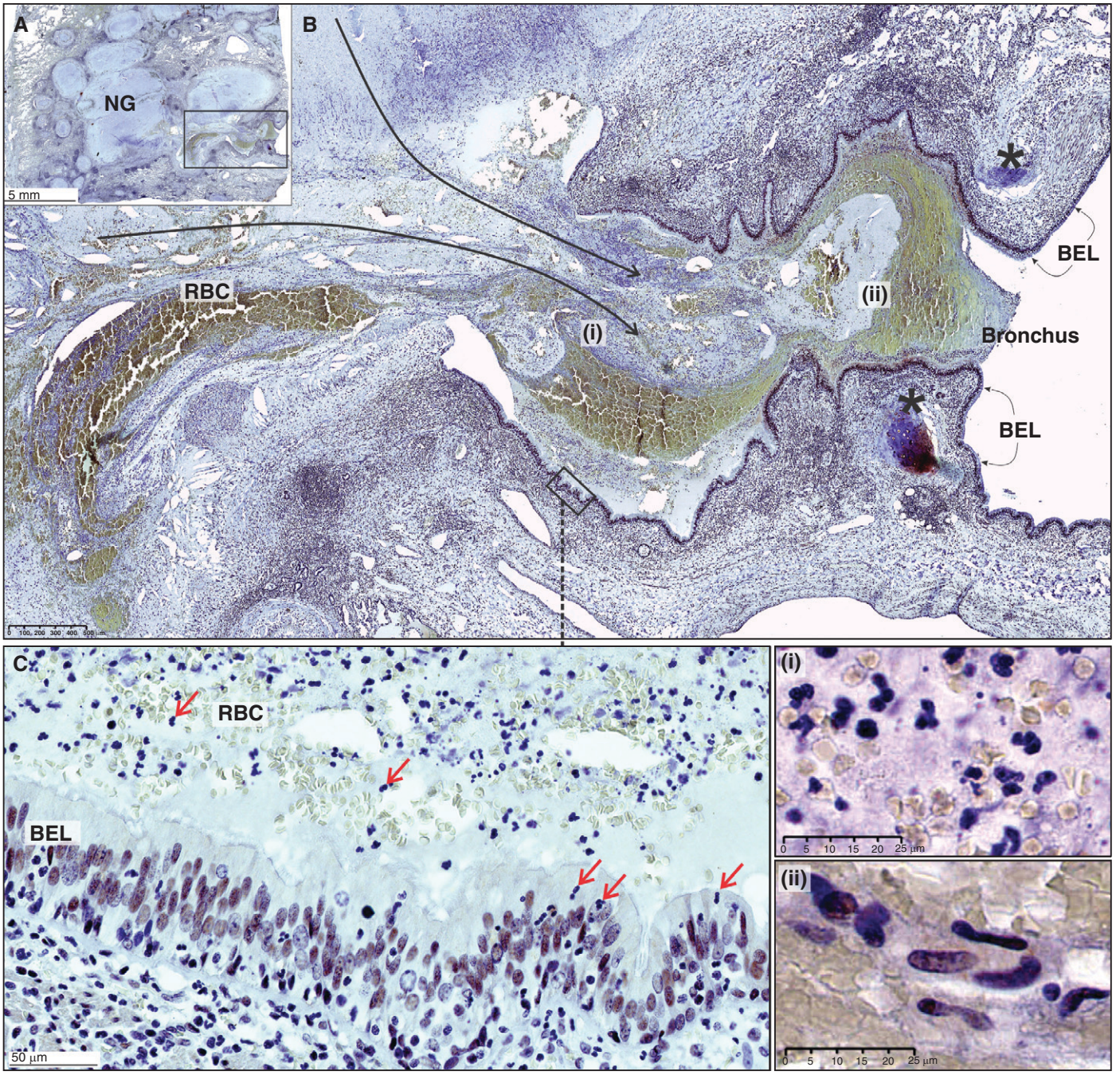

Figure 7. Bronchial obstruction of a *Mycobacterium tuberculosis*–infected human lung. (*A*) Low-power magnification of acid sphingomyelinase (nuclear) staining. Note the spilling of necrotic material from necrotic granulomas (NGs) into an airway. These NGs are surrounded by foam cells (*see* Figure E11 in the online supplement). (*B*) Medium-power image (black asterisks indicate cartilage, and long black arrows indicate spillage of necrotic material into the bronchus) of the boxed area in *A*. (*C*) High-power depiction of the bronchial epithelial layer (BEL) with immune cells in the airway (boxed area in *B*). Red arrows indicate neutrophils in the lumen and BEL. (*i*) High-power depiction of immune cells, nuclear debris, and RBC in the necrotic lumen. (*ii*) High-power depiction of epithelioid histiocytes in the necrotic lumen. Scale bars: *A*, 5 mm; *B*, 500 μm; *C*, 50 μm; *i* and *ii*, 25 μm. RBC = red blood cells.

identification of a TB "lesion" (15), which is distinct from granulomas in this study.

Third, our findings highlight the pathophysiological factors that influence the shape of the granuloma. It is evident that immune-cell infiltration in the alveoli, bronchioles, and bronchi dictate lesion shape and that immune-cell recruitment and subsequent necrosis expand in the airways by following "the path of least resistance." Alveolar walls contain numerous interalveolar pores that may enable dissemination of *M. tuberculosis* or infected cells. The complex 3D morphology of granulomas is reminiscent of the tree-in-bud form, an HRCT signature that

is present in cases of active pulmonary TB and is indicative of bronchial obstruction (12, 18, 34). Studies in humans and nonhuman primates have shown that individual TB lesions follow distinct and overlapping trajectories, suggesting that local factors dictate lesion formation (35). Consistent with the results of autopsy studies (36), our findings show that necrotic material fills the bronchiolar lumen to induce further bronchial wall necrosis.

The spatial relationship between TB lesions and the surrounding vasculature sheds light on the complex pathophysiology involved in promoting drug tolerance. For example, 3D segmentation of the vasculature from TB lungs shows destruction of the vascular network, which would reduce delivery of bactericidal concentrations of drugs (37), nutrients, immune cells, and O_2. Because obstructed airways are not vascularized, they provide a safe haven for drug-tolerant *M. tuberculosis*, which may further disseminate via accumulation of inflammatory cells in the airway network. Hence, it is reasonable to posit that dissemination of *M. tuberculosis* from obstructed bronchioles to other areas of the lung explains how new lesions are formed in patients after anti-TB treatment (15). Classical and more recent radiological studies have shown that adult-type or post-primary TB was known as bronchogenic TB because *M. tuberculosis* disseminates through the bronchi rather than via the lymphatics or the bloodstream (16–19, 38). Lastly, Canetti (2) posited that bronchogenic spread in cavitary patients is very slow because the immune system is very effective against small numbers of *M. tuberculosis* bacilli but is ineffective when a certain threshold is breached. Not surprisingly, rest therapy was proposed as a means to reduce the amplitude and frequency of pulmonary movements to limit *M. tuberculosis* dispersion.

Our findings also have implications for understanding the drug tolerance and persistence of *M. tuberculosis* in O_2-deficient lesions. The maximum O_2 diffusion distance is 200 μm (22–24), beyond which tissue becomes hypoxic. Necrotic lesions in some animal models of TB have been shown to be hypoxic (39). By measuring the distance between blood vessels and the segmented TB lesions, our findings support these studies showing that some necrotic granulomas in humans are hypoxic. On the basis of a recent study (25), it is likely that gradients of drugs, metabolites, and O_2 exist within TB lung tissue. Therefore, separate anisotropic gradients for different drugs (40) may trigger sequential development of drug resistance by passaging through environments with low drug concentrations. Hence, therapeutic angiogenesis (37) and aerosolized drug delivery strategies (33) may represent plausible approaches to increase anti-TB drug concentrations in the granuloma.

Our study has some limitations. First, a limited number of lung tissue samples were examined from patients with TB with diverse medical histories and treatments; hence, it is likely that a larger test cohort may render a more representative disease spectrum. However, sampling from different regions of each lung allowed us to evaluate microenvironments at different stages of tissue pathology. In addition, similar to what is seen in conventional histopathology, shrinkage of tissue during formalin fixation and staining is unavoidable. Lastly, because we analyzed lung tissue from patients with TB suffering from severe disease, these results may not represent more moderate manifestations of TB.

Overall, our findings have important implications for TB disease treatment because several surprising findings were made, including that there is spectrum of granuloma 3D structures, that granulomas are shaped by bronchi, that granulomas have a spatial organization in relation to the vasculature and airways, and that obstructive bronchi are used as a conduit for *M. tuberculosis* dissemination in the lung (i.e., bronchogenic spread). ■

Author disclosures are available with the text of this article at www.atsjournals.org.

Acknowledgment: The authors thank Dr. P. K. Ramdial at Lancet Laboratories, Durban, South Africa, for the invaluable contribution and thank all staff in the Africa Health Research Institute (AHRI) clinical core.

References

1. Rich AR. The pathogenesis of tuberculosis. Baltimore, MD: C. C. Thomas; 1944.
2. Canetti G. The tubercle bacillus in the pulmonary lesion of man: histobacteriology and its bearing on the therapy of pulmonary tuberculosis. New York, NY: Springer; 1955.
3. Silva Miranda M, Breiman A, Allain S, Deknuydt F, Altare F. The tuberculous granuloma: an unsuccessful host defence mechanism providing a safety shelter for the bacteria? *Clin Dev Immunol* 2012;2012:139127.
4. Gil O, Díaz I, Vilaplana C, Tapia G, Díaz J, Fort M, *et al.* Granuloma encapsulation is a key factor for containing tuberculosis infection in minipigs. *PLoS One* 2010;5:e10030.
5. Marino S, El-Kebir M, Kirschner D. A hybrid multi-compartment model of granuloma formation and T cell priming in tuberculosis. *J Theor Biol* 2011; 280:50–62.
6. Ordonez AA, Pokkali S, DeMarco VP, Klunk M, Mease RC, Foss CA, *et al.* Radioiodinated DPA-713 imaging correlates with bactericidal activity of tuberculosis treatments in mice. *Antimicrob Agents Chemother* 2015;59: 642–649.
7. Prats C, Vilaplana C, Valls J, Marzo E, Cardona PJ, López D. Local inflammation, dissemination and coalescence of lesions are key for the progression toward active tuberculosis: the bubble model. *Front Microbiol* 2016;7:33.
8. Hao W, Schlesinger LS, Friedman A. Modeling granulomas in response to infection in the lung. *PLoS One* 2016;11:e0148738.
9. Pienaar E, Sarathy J, Prideaux B, Dietzold J, Dartois V, Kirschner DE, *et al.* Comparing efficacies of moxifloxacin, levofloxacin and gatifloxacin in tuberculosis granulomas using a multi-scale systems pharmacology approach. *PLOS Comput Biol* 2017;13:e1005650.
10. Goldberg MF, Roeske EK, Ward LN, Pengo T, Dileepan T, Kotov DI, *et al.* Salmonella persist in activated macrophages in T cell-sparse granulomas but are contained by surrounding CXCR3 ligand-positioned Th1 cells. *Immunity* 2018;49:1090–1102.e7.
11. Lin PL, Flynn JL. CD8 T cells and *Mycobacterium tuberculosis* infection. *Semin Immunopathol* 2015;37:239–249.
12. Hunter RL. Tuberculosis as a three-act play: a new paradigm for the pathogenesis of pulmonary tuberculosis. *Tuberculosis (Edinb)* 2016;97: 8–17.
13. Yeh JJ, Yu JK, Teng WB, Chou CH, Hsieh SP, Lee TL, *et al.* High-resolution CT for identify patients with smear-positive, active pulmonary tuberculosis. *Eur J Radiol* 2012;81:195–201.
14. Lee SW, Jang YS, Park CM, Kang HY, Koh WJ, Yim JJ, *et al.* The role of chest CT scanning in TB outbreak investigation. *Chest* 2010;137:1057–1064.
15. Malherbe ST, Shenai S, Ronacher K, Loxton AG, Dolganov G, Kriel M, *et al.*; Catalysis TB–Biomarker Consortium. Persisting positron emission tomography lesion activity and *Mycobacterium tuberculosis* mRNA after tuberculosis cure. *Nat Med* 2016;22:1094–1100.
16. Kayne GG. Origin, diagnosis, and management of early bronchogenic tuberculosis. Br Med J 1941;2:154–152.

17. Pagel W. An outline of the principal forms of tuberculosis in man; primary, disseminated and bronchogenic tuberculosis. *Postgrad Med J* 1952;28: 606.
18. Im JG, Itoh H, Lee KS, Han MC. CT-pathology correlation of pulmonary tuberculosis. *Crit Rev Diagn Imaging* 1995;36:227–285.
19. Skoura E, Zumla A, Bomanji J. Imaging in tuberculosis. *Int J Infect Dis* 2015; 32:87–93.
20. Chinta KC, Rahman MA, Saini V, Glasgow JN, Reddy VP, Lever JM, *et al.* Microanatomic distribution of myeloid heme oxygenase-1 protects against free radical-mediated immunopathology in human tuberculosis. Cell Rep 2018;25:1938–1952, e5.
21. Reddy VP, Chinta KC, Saini V, Glasgow JN, Hull TD, Traylor A, *et al.* Ferritin H deficiency in myeloid compartments dysregulates host energy metabolism and increases susceptibility to *Mycobacterium tuberculosis* infection. *Front Immunol* 2018;9:860.
22. Dewhirst MW, Secomb TW, Ong ET, Hsu R, Gross JF. Determination of local oxygen consumption rates in tumors. *Cancer Res* 1994;54:3333–3336.
23. Olive PL, Vikse C, Trotter MJ. Measurement of oxygen diffusion distance in tumor cubes using a fluorescent hypoxia probe. *Int J Radiat Oncol Biol Phys* 1992;22:397–402.
24. Thomlinson RH, Gray LH. The histological structure of some human lung cancers and the possible implications for radiotherapy. *Br J Cancer* 1955; 9:539–549.
25. Kumar S, Sharife H, Kreisel T, Mogilevsky M, Bar-Lev L, Grunewald M, *et al.* Intra-tumoral metabolic zonation and resultant phenotypic diversification are dictated by blood vessel proximity. *Cell Metab* 2019;30: 201–211, e6.
26. Rahman MA, Cumming BM, Addicott K, Pac IH, Russell S, Nargan K, *et al.* Hydrogen sulfide dysregulates the immune response by suppressing central carbon metabolism to promote tuberculosis. *Proc Natl Acad Sci USA* 2020;117:6663–6674.
27. Hunter RL. The pathogenesis of tuberculosis. The early infiltrate of post-primary (adult pulmonary) tuberculosis: a distinct disease entity. *Front Immunol* 2018;9:2108.
28. Medlar EM. Primary and reinfection tuberculosis as the cause of death in adults; an analysis of 100 consecutive necropsies. *Am Rev Tuberc* 1947; 55:517–528.
29. Medlar EM. Pathogenetic concepts of tuberculosis. *Am J Med* 1950;9:611–622.
30. Esmail H, Lai RP, Lesosky M, Wilkinson KA, Graham CM, Coussens AK, *et al.* Characterization of progressive HIV-associated tuberculosis using 2-deoxy-2-[^{18}F]fluoro-D-glucose positron emission and computed tomography. *Nat Med* 2016;22:1090–1093.
31. Esmail H, Lai RP, Lesosky M, Wilkinson KA, Graham CM, Horswell S, *et al.* Complement pathway gene activation and rising circulating immune complexes characterize early disease in HIV-associated tuberculosis. *Proc Natl Acad Sci USA* 2018;115:E964–E973.
32. Diedrich CR, O'Hern J, Wilkinson RJ. HIV-1 and the *Mycobacterium tuberculosis* granuloma: a systematic review and meta-analysis. *Tuberculosis (Edinb)* 2016;98:62–76.
33. Braunstein M, Hickey AJ, Ekins S. Why wait? The case for treating tuberculosis with inhaled drugs. *Pharm Res* 2019;36:166.
34. Im J-G, Itoh H. Tree-in-bud pattern of pulmonary tuberculosis on thin-section CT: pathological implications. *Korean J Radiol* 2018;19:859–865.
35. Lin PL, Ford CB, Coleman MT, Myers AJ, Gawande R, Ioerger T, *et al.* Sterilization of granulomas is common in active and latent tuberculosis despite within-host variability in bacterial killing. *Nat Med* 2014;20:75–79.
36. Im JG, Itoh H, Shim YS, Lee JH, Ahn J, Han MC, *et al.* Pulmonary tuberculosis. CT findings: early active disease and sequential change with antituberculous therapy. *Radiology* 1993;186:653–660.
37. Oehlers SH, Cronan MR, Scott NR, Thomas MI, Okuda KS, Walton EM, *et al.* Interception of host angiogenic signalling limits mycobacterial growth. *Nature* 2015;517:612–615.
38. Rich AR. The pathogenesis of tuberculosis. Baltimore, MD: C. C. Thomas; 1951.
39. Via LE, Lin PL, Ray SM, Carrillo J, Allen SS, Eum SY, *et al.* Tuberculous granulomas are hypoxic in guinea pigs, rabbits, and nonhuman primates. *Infect Immun* 2008;76:2333–2340.
40. Prideaux B, Via LE, Zimmerman MD, Eum S, Sarathy J, O'Brien P, *et al.* The association between sterilizing activity and drug distribution into tuberculosis lesions. *Nat Med* 2015;21:1223–1227.
41. Wells G, Glasgow JN, Nargan K, Lumamba K, Madansein R, Maharaj K, *et al.* 3D microarchitecture of the human tuberculous granuloma [preprint]. bioRxiv; 2020 [accessed 2021 Aug 19]. Available from: https://www.biorxiv.org/content/10.1101/2020.06.14.149898v1.